JACS
JOURNAL OF THE AMERICAN CHEMICAL SOCIETY
Article
pubs.acs.org/JACS

Visible-Light Photoexcited Electron Dynamics of Scandium Endohedral Metallofullerenes: The Cage Symmetry and Substituent Effects

Bo Wu,[†,∥] Jiahua Hu,[§,∥] Peng Cui,[§,∥] Li Jiang,[†] Zongwei Chen,[§] Qun Zhang,*[,§] Chunru Wang,*[,†] and Yi Luo*[,§,‡]

[†]Laboratory of Molecular Nanostructure and Nanotechnology, Institute of Chemistry, Beijing National Laboratory for Molecular Sciences, Beijing 100190, China

[§]Hefei National Laboratory for Physical Sciences at the Microscale, Department of Chemical Physics, Synergetic Innovation Center of Quantum Information and Quantum Physics, University of Science and Technology of China, Hefei, Anhui 230026, China

[‡]Department of Theoretical Chemistry, School of Biotechnology, Royal Institute of Technology, AlbaNova, S-106 91 Stockholm, Sweden

Supporting Information

ABSTRACT: Endohedral metallofullerenes (EMFs) have become an important class of molecular materials for optoelectronic applications. The performance of EMFs is known to be dependent on their symmetries and characters of the substituents, but the underlying electron dynamics remain unclear. Here we report a systematic study on several scandium EMFs and representative derivatives to examine the cage symmetry and substituent effects on their photoexcited electron dynamics using ultrafast transient absorption spectroscopy. Our attention is focused on the visible-light (530 nm as a demonstration) photoexcited electron dynamics, which is of broad interest to visible-light solar energy harvesting but is considered to be quite complicated as the visible-light photons would promote the system to a high-lying energy region where dense manifolds of electronic states locate. Our ultrafast spectroscopy study enables a full mapping of the photoinduced deactivation channels involved and reveals that the long-lived triplet exciton plays a decisive role in controlling the photoexcited electron dynamics under certain conditions. More importantly, it is found that the opening of the triplet channels is highly correlated to the fullerene cage symmetry as well as the electronic character of the substituents.

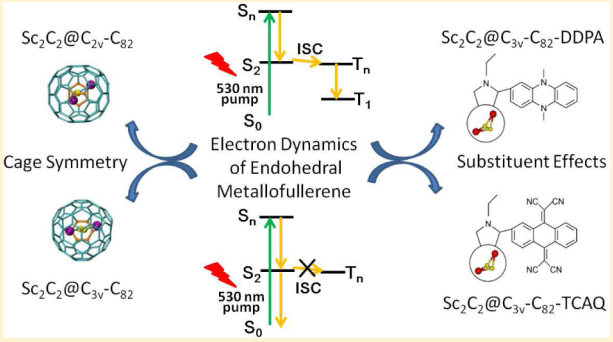

INTRODUCTION

Endohedral metallofullerenes (EMFs) are constructed by fullerenes encapsulating one or more metal atoms in their interior.[1−10] Recently, a variety of EMFs have been integrated into various photoactive conjugates or hybrids, giving rise to distinctive photophysical behaviors.[11−13] Particularly, the unique physicochemical properties and rich electrochemical properties of EMFs relate to the significant hybridization effect of the encapsulated metallic cluster.[14,15] Their ground- and excited-state features largely depend on the nature as well as the composition of the encapsulated species.[16] A number of covalently linked electron donor−acceptor conjugates have also been developed to mimic photosynthesis and to realize optoelectronic devices.[17,18] Efforts have been made to look into the mechanistic details concerning the charge-transfer events in these electron donor−acceptor conjugates and the fate of the subsequently formed radical ion pair states.[19] For example, when electron acceptors such as 11,11,12,12-tetracyano-9,10-anthra-*p*-quinodimethane (TCNQ) and 1,6,7,12-tetrachloro-3,4,9,10-perylenediimide (PDI) or electron donor 9,10-bis(1,3-dithiol-2-ylidene)-9,10-dihydroanthracene (exTTF) are linked to EMFs via a flexible σ-spacer or a pyrrolidine ring, they exhibit higher photocurrent efficiency or electron mobility.[20,21] Such kinds of remarkable chemical and physical features have inspired chemists to design and synthesize novel derivatives of EMFs as building blocks for optoelectronic materials.[22−26]

Herein, we address the interesting yet unexploited issues about how the point group symmetry of the EMFs cage as well as the electronic character of different substituents (i.e., the EMFs cage modified by electron-acceptor or -donor groups) subtly affect the visible-light photoexcited electron dynamics involved. Notably, such unique carbide cluster metallofullerenes have become the second largest sub-branch of cluster EMFs. Ultrafast transient absorption (TA) spectroscopy, a robust tool for tracking in real time electron dynamics in molecular systems,[27] is used to examine the photoexcited electron dynamics of three isomers of $Sc_2C_2@C_{82}$ with different cage

Received: April 11, 2015
Published: June 22, 2015

DOI: 10.1021/jacs.5b03612
J. Am. Chem. Soc. 2015, 137, 8769−8774

symmetries (i.e., C_s, C_{2v}, and C_{3v}) and two representative $Sc_2C_2@C_{3v}$-C_{82} derivatives.

RESULTS AND DISCUSSION

Preparation of Metallofullerenes. The target molecules $Sc_2C_2@C_s$-C_{82}, $Sc_2C_2@C_{2v}$-C_{82}, and $Sc_2C_2@C_{3v}$-C_{82} are synthesized by the Kräschmer–Huffman arc discharging method[28] and isolated using the multistage high-performance liquid chromatography (HPLC). The purity of our samples is confirmed by the HPLC analysis, the matrix assisted laser desorption ionization/time-of-flight (MALDI-TOF) mass spectrometry, and the UV–vis-NIR spectra (see Supporting Information for details). The detailed information about the geometrical structures and electronic properties of the $Sc_2C_2@C_{82}$ isomers has been reported.[29−35] By comparing the spectral fingerprints in the measured UV–vis-NIR absorption spectra of each isolated $Sc_2C_2@C_{82}$ isomer with those known $Sc_2C_2@C_{82}$ isomers and the typical retention times of them in chromatography, we can thus unambiguously distinguish the correct $Sc_2C_2@C_{82}$ isomers one by one. The insets of Figure 1a (on the right-hand side) depict the optimized structures of the three isomers of $Sc_2C_2@C_{82}$; the relevant computational details are given in Supporting Information.

The Cage Symmetry-Dependent Excited-State Dynamics Process. In our ultrafast TA measurements, a femtosecond visible pump/white-light continuum (WLC) probe scheme is employed; the details of the pump–probe experiments are given in Supporting Information. The center wavelength of pump pulses is chosen at 530 nm (ca. 2.34 eV), which is suited to promote the scandium fullerene molecule from its electronic ground state S_0 to a certain high-lying, electronically excited state S_n. Since the 400–700 nm WLC probe yields essentially the same TA kinetics, we show here a set of representative data taken at 470 nm (Figure 1a). Remarkably, the C_s and C_{3v} isomers exhibit similar relaxation kinetics, while the C_{2v} isomer behaves quite differently. The former two isomers feature an initial, rapid buildup of TA signal, followed by a biexponential decay with similar time constants: τ_1 = 4.7 ± 0.3 ps and τ_2 = 67 ± 4 ps for the C_s isomer; τ_1 = 3.1 ± 0.1 ps and τ_2 = 59 ± 4 ps for the C_{3v} isomer. For the C_{2v} isomer, however, its relaxation is found to be characterized by three time constants: τ_1 = 4.7 ± 1.4 ps, τ_2 = 138 ± 31 ps, and τ_3 > 3.6 ± 1.1 ns.

To understand the above cage symmetry-dependent relaxation kinetics, we resort to the assistance from the first-principles calculations on the relevant electronically excited states, including the singlet (S_1 up to S_n) and triplet (T_1 up to T_n) states lying around and below the 530 nm photon energy of ca. 2.34 eV, as displayed in Figure 1b. The related corresponding excitation energies and main orbital transition configurations are summarized in Table S2, Supporting Information. Here, care must be taken in the following three facts: (i) The cascading internal conversion (IC) processes from S_n to lower singlet states (normally S_1) are much more effective than the intersystem crossing (ISC) processes that bridge the population transfer from the singlet space to the triplet space, as dictated by the well-known Kasha's rule,[36] (ii) generally, the smaller the energy separation between S_2 and S_1, the larger the IC ($S_2 \rightarrow S_1$) rate; and (iii) given that the low-lying singlet states (normally S_2 and/or S_1) locate quite close to a certain triplet state (better degenerate in energy for such S–T pair), the ISC probability can usually get significantly enhanced.[37] With these facts in mind, one can immediately

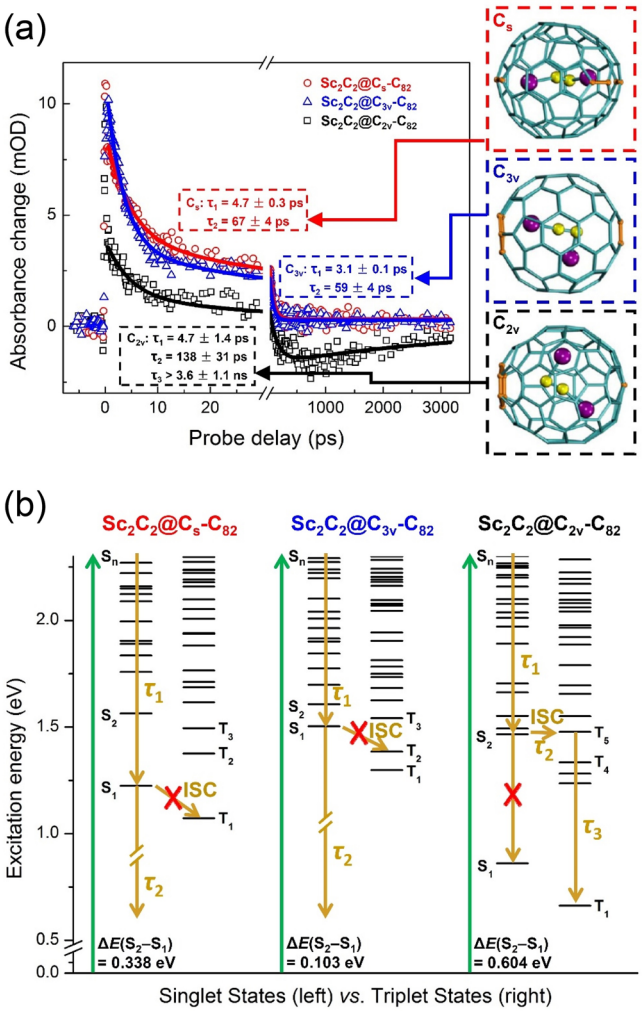

Figure 1. (a) Representative TA kinetics (probed at 470 nm) for the three isomers of $Sc_2C_2@C_{82}$ with different cage symmetries (i.e., C_s, C_{2v}, and C_{3v}). The pump wavelength is 530 nm. The TA signal (i.e., absorbance change) is given in mOD, where OD stands for optical density. The insets (right-hand side) show the optimized structures of the three types of $Sc_2C_2@C_{82}$. The carbon atoms defining the cage symmetry are highlighted by orange color, while the other carbon atoms on the cage are shown as a cyan framework. The inner Sc and C atoms are shown by purple and yellow colors, respectively. (b) The relevant mechanisms for the two types of TA kinetics observed; see text for relevant discussions.

understand the physical picture of what is schematically illustrated in Figure 1b.

For the C_s and C_{3v} isomers, the time constants τ_1 and τ_2 can be ascribed to the two consecutive relaxation processes of $S_n \rightarrow S_1$ and $S_1 \rightarrow S_0$, respectively. Due to the relatively large energy separation of the relevant S–T pair, the ISC processes are ineffective in the two cases. In the C_{2v} isomer case, however, the unique distribution of electronic states, i.e., the existence of nearly degenerate S_2–T_5 pair as well as the largest energy separation between S_2 and S_1 (as compared to the other two isomers), renders the S_2 state an effective "stop" of population flow along the cascading IC ($S_n \rightarrow S_1$). As such, the two-step relaxation in the other two isomers turns into a three-step one: τ_1 (ca. 4.7 ps) describes the fast IC ($S_n \rightarrow S_2$) process, while τ_2 (ca. 138 ps) describes the effective ISC ($S_2 \rightarrow T_5$) process and τ_3 (>3.6 ns) describes the subsequent relaxation processes in

DOI: 10.1021/jacs.5b03612
J. Am. Chem. Soc. 2015, 137, 8769–8774

the triplet space starting from the T_5 state, as annotated in Figure 1b.

On the basis of the above observations and analysis, it is evident that the long-lived triplet excitons can be achieved in scandium fullerenes by simply altering the point group symmetry of the hollow fullerene cage. Notably, the C_{2v} isomer has the smallest HOMO−LUMO gap (Figure 2), which implies

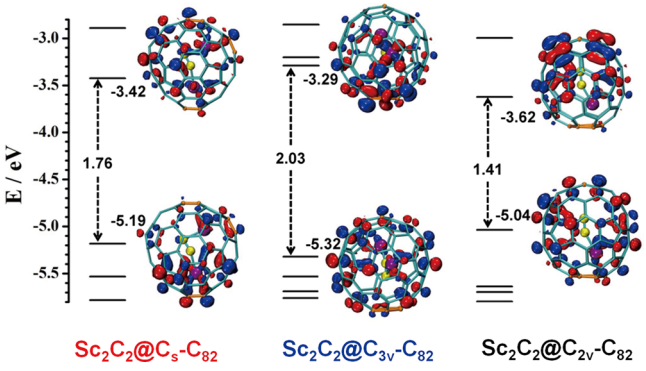

Figure 2. Energy levels (in eV) for the three isomers of $Sc_2C_2@C_{82}$ with different cage symmetries. HOMOs and LUMOs are shown with isovalues being ±0.03.

the low stability of the singlet ground state and the relatively high stability of triplet excited states. Also, from Figure 2 one can see that the HOMO and LUMO are mainly situated on the carbon atoms of the fullerene cage. The excited states under investigation are contributed mainly by the electronic structure of fullerene carbon cage, which is determined by the distribution of the pentagons and hexagons (the latter could be reflected and characterized by the cage symmetry). This explains, to a certain extent, why the observed TA kinetics of the carbide cluster EMFs is dependent on the cage symmetry, although the totally same carbide cluster is encapsulated in. On the other hand, however, the encapsulated Sc_2C_2 cluster is indispensable: Apart from providing electrons to the carbon cage to make the cage stable, the metal atoms may enhance the ISC coupling between different spin states of the carbon cage, which could be inferred from the HOMO and LUMO distributions (Figure 2) where the metal atoms are close enough to the molecular orbitals because of the trap by the closed carbon cage.

We also notice that NMR spectroscopy has been used to investigate the dynamics of Sc_2C_2 unit in the ^{13}C-enriched $Sc_2C_2@C_{3v}$-C_{82}.[35] When temperature is increased, the signal of the carbon atoms in the interior C_2 unit exhibits considerable broadening as a result of the spin−rotation relaxation effect.[35] Similar broadening and temperature-dependent shifts of the signals corresponding to the carbon atoms of the C_2 unit are also reported for the $Sc_2C_2@C_s$-C_{82}.[29] The ^{13}C NMR line widths of C_2 inside the $Sc_2C_2@C_s$-C_{82} and the $Sc_2C_2@C_{3v}$-C_{82} are 20 and 30 at 293 K, respectively, but the $Sc_2C_2@C_{2v}$-C_{82} is found to exhibit a sharp ^{13}C NMR peak of the C_2 signal.[38] Moreover, it is noted that the Sc_2C_2 cluster is C_1-symmetric when it is inside the $Sc_2C_2@C_s$-C_{82} and $Sc_2C_2@C_{3v}$-C_{82}, while it becomes C_s-symmetric in $Sc_2C_2@C_{2v}$-C_{82}; thus, it is understandable that the rotation of C_2 inside the C_{2v} isomer is easier than that inside the C_s and C_{3v} isomers. As the electronic transmission needs to cross a high barrier, the excited electrons can be easily transferred from the carbon cage to the interior metal cluster for the C_{2v} isomer than the other two. Consequently, the spin−obit coupling between different excited states could be enhanced in the $Sc_2C_2@C_{2v}$-C_{82}, achieving longer-lived triplet excitons therein, as also verified by our ultrafast TA measurements.

The Substituent-Dependent Excited-State Dynamics Process. Further, we have examined how the visible-light photoexcited electron dynamics of interest vary when two types of organic groups (i.e., electron acceptor or electron donor) are engrafted onto the hollow fullerene cage. Presented here is an illustrative case study on the C_{3v} isomer. We synthesize the target molecules $Sc_2C_2@C_{3v}$-C_{82}-2,2′-(anthracene-9,10-diylidene)dimalononitrile ($Sc_2C_2@C_{3v}$-C_{82}-TCAQ; electron acceptor-modified case) and $Sc_2C_2@C_{3v}$-C_{82}-5,10-dimethyl-5,10-dihydrophenazine ($Sc_2C_2@C_{3v}$-C_{82}-DDPA; electron donor-modified case), whose structures are depicted in Figure 3a. The synthesis follows the procedures of 1,3-dipolar

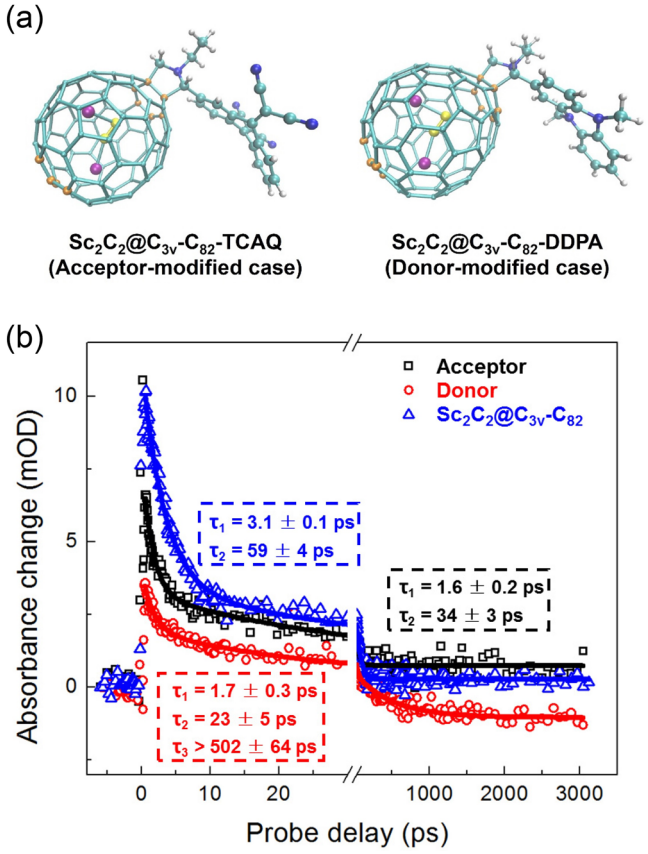

Figure 3. Structures of $Sc_2C_2@C_{3v}$-C_{82}-TCAQ (electron acceptor-modified case) and $Sc_2C_2@C_{3v}$-C_{82}-DDPA (electron donor-modified case). (b) Representative TA kinetics (probed at 470 nm) for the unmodified $Sc_2C_2@C_{3v}$-C_{82} (from Figure 1a; given here for comparison), the electron acceptor-modified $Sc_2C_2@C_{3v}$-C_{82}-TCAQ, and the electron donor-modified $Sc_2C_2@C_{3v}$-C_{82}-DDPA. The pump wavelength used is 530 nm. The TA signal (i.e., absorbance change) is given in mOD, where OD stands for optical density.

cycloaddition reactions, in which the reactive azomethine ylides are generated from the aminoacetic acids and the aldehydes react with the $Sc_2C_2@C_{3v}$-C_{82}. Details of the syntheses, isolations, purifications, and electrochemical studies of the two representatives $Sc_2C_2@C_{3v}$-C_{82} derivatives are introduced in the Supporting Information. Since previous study on similar Prato reaction has unambiguously determined the structure of the $Sc_2C_2@C_{3v}(8)$-C_{82} derivative by the single-crystal X-ray

DOI: 10.1021/jacs.5b03612
J. Am. Chem. Soc. 2015, 137, 8769−8774

crystallography,[39] the two metallofullerene derivatives are suggested to own similar geometric structures with the addition sites locating on the [6,6]-bond junction in the metallofullerene cage.

It turns out that the engraftment of electron acceptor can barely alter the TA kinetics. Both the C_{3v} isomer and its electron acceptor-engrafted counterpart exhibit biexponential decay with more or less the same time constants, as annotated in Figure 3b. In contrast, the engraftment of electron donor brings about dramatic change. The relaxation kinetics can only be fitted with more than three exponential components. Since the final recovery (to zero absorbance change) is beyond the detection limit (ca. 3.2 ns) of our pump−probe spectrometer, only three exponential components can be given, as annotated in Figure 3b.

To help understand the pertinent mechanisms for the above observations, we collect and compare the calculated distributions of the relevant electronically excited states in Figure 4. For

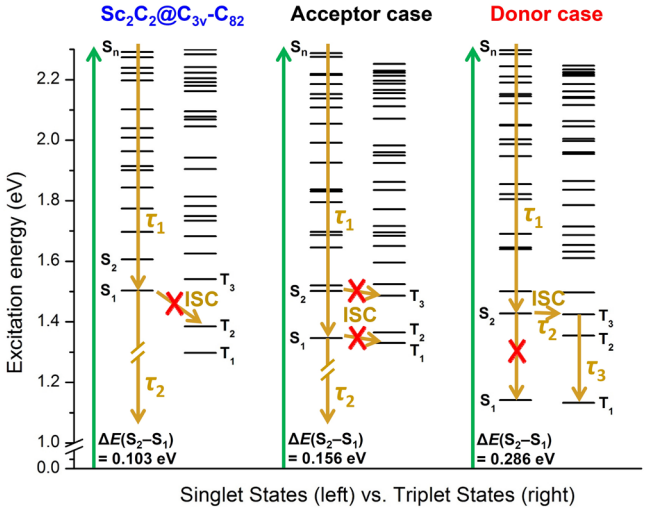

Figure 4. Relevant mechanisms for the two types of TA kinetics observed in the electron acceptor-modified and the electron donor-modified cases, as annotated in the plot; see text for relevant discussions.

the donor-modified case, the existence of nearly degenerate S_2−T_3 pair as well as the largest energy separation between S_2 and S_1 (as compared to the other two cases shown in Figure 4) renders the S_2 state a "stop" of population flow along the cascading IC ($S_n \rightarrow S_1$), similarly to the C_{2v} isomer case discussed above (refer to Figure 1b). As such, here a three-step relaxation kinetics is observed again: τ_1 (ca. 1.7 ps) describes the fast IC ($S_n \rightarrow S_2$) process, τ_2 (ca. 23 ps) describes the very effective ISC ($S_2 \rightarrow T_3$) process, and τ_3 (>502 ps) describes the subsequent relaxation processes in the triplet space starting from the T_3 state, as annotated in Figure 4.

Apparently, a question arises with the acceptor-modified case: Albeit the S_2−T_3 and S_1−T_1 pairs are not as degenerate as in the donor-modified case, they are obviously fairly close to each other in energy, so, why are the corresponding ISC ($S_2 \rightarrow T_3$) and ISC ($S_1 \rightarrow T_1$) processes ineffective in the acceptor-modified case? To answer this question, we interrogate the molecular orbital profiles that correspond to electronic transitions with the relevant singlet (S_2 and S_1) and triplet (T_3 and T_1) states for both the acceptor-modified and donor-modified cases, as shown in Figure 5.

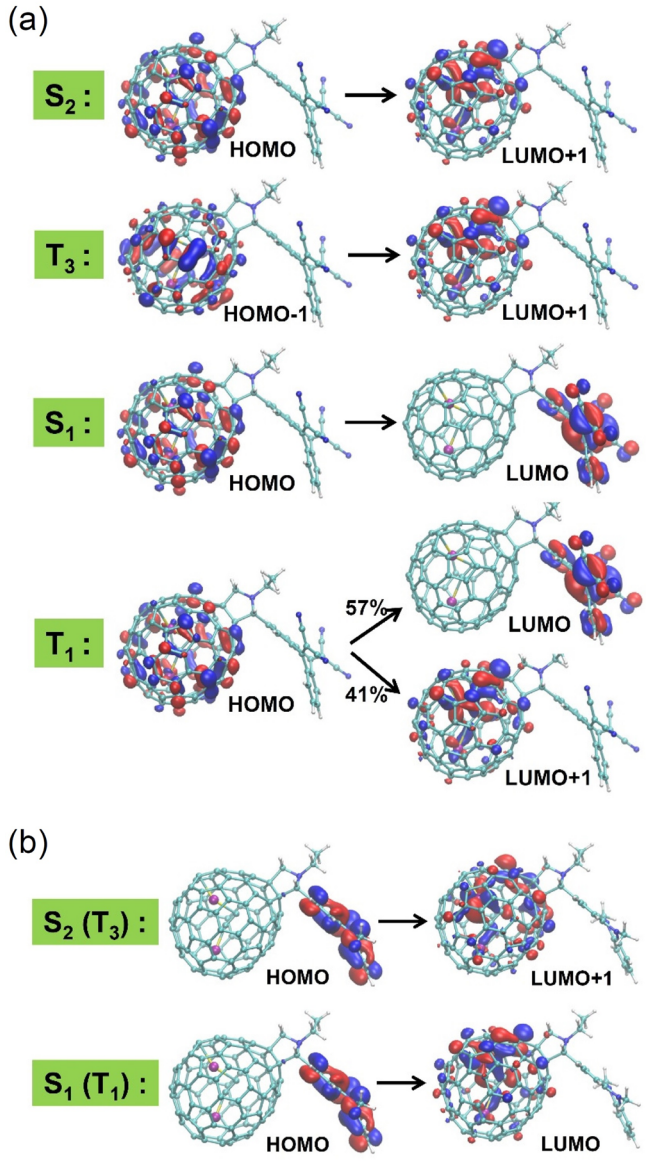

Figure 5. Molecular orbital profiles corresponding to electronic transitions with the relevant singlet (S_2 and S_1) and triplet (T_3 and T_1) states for (a) the $Sc_2C_2@C_{3v}$-C_{82}-TCAQ (electron acceptor-modified) case and (b) the $Sc_2C_2@C_{3v}$-C_{82}-DDPA (electron donor-modified) case.

Information for more related electronically excited states can be found in Table S3, Supporting Information. For the acceptor-modified case (Figure 5a), both the S_2−T_3 and S_1−T_1 pairs correspond to different orbital transition types [i.e., HOMO → LUMO+1 for S_2 while HOMO−1 → LUMO+1 for T_3; HOMO → LUMO for S_1 while HOMO → LUMO (57%) plus HOMO → LUMO+1 (41%) for T_1]. Such different orbital transition types, which give rise to the corresponding singlet and triplet states, could play a decisive role in impeding the ISC processes despite the fact that the energy separations of the nearby S−T pairs are fairly small. In contrast, for the donor-modified case (Figure 5b), however, both the S_2−T_3 and S_1−T_1 pairs correspond to the same orbital transition types (i.e., HOMO → LUMO+1 for both S_2 and T_3 while HOMO → LUMO for both S_1 and T_1), which could be rather advantageous for enhancing the corresponding ISC ($S_2 \rightarrow T_3$) and ISC ($S_1 \rightarrow T_1$) processes. Here, it is worth noting that

DOI: 10.1021/jacs.5b03612
J. Am. Chem. Soc. 2015, 137, 8769−8774

the quite effective ISC ($S_2 \rightarrow T_3$) process ($\tau_2 \sim 23$ ps) plus the largest energy separation between S_2 and S_1 (as compared to the other two cases shown in Figure 4) make the IC ($S_2 \rightarrow S_1$) process much less competitive than the ISC ($S_2 \rightarrow T_3$) process, and hence it is unnecessary to take into account the possible ISC ($S_1 \rightarrow T_1$) process which could be effective if occurs.

In addition, for the donor-modified case, it is found that up until 3 ns (near the detection limit of our pump−probe spectrometer) there is still no trend of TA recovery (to zero absorbance change) at all. This implies that the relaxation process in the triplet space of the donor-modified $Sc_2C_2@C_{3v}$-C_{82} molecule is extremely slow; a process can presumably be described by one (or more) unmeasurable time constant(s), e.g., τ_4 or others.

Based upon the above observations of substituent effect, we can safely conclude that it is also possible to achieve long-lived triplet excitons in EMFs by simply engrafting electron-donor group onto the hollow fullerene cage of EMFs. Such long-lived triplet excitons could play a decisive role in controlling the population or energy-transfer processes of the system. Evidently, the opening of the triplet channels is highly correlated not only to the cage symmetry (as verified before; Figures 1 and 2) but also to the electron character of the substituents (as verified here; Figures 3−5).

CONCLUSION

To summarize, by means of ultrafast transient absorption spectroscopy we have for the first time revealed the subtle cage symmetry and substituent effects on the visible-light (530 nm as a demonstration) photoexcited electron dynamics of several scandium endohedral metallofullerenes and representative derivatives. This systematic study is expected to pave the way toward achieving the desirable long-lived triplet excitons in many endohedral metallofullerenes by engineering the point group symmetry of the hollow fullerene cage or by modifying the fullerene cage with externally engrafted groups. We also envision that the understanding gained from this work could provide valuable guidance for potential applications of endohedral metallofullerene molecular systems in visible-light solar energy harvesting.

ASSOCIATED CONTENT

Supporting Information

Details of the sample preparation and characterizations, the femtosecond pump−probe experiments, and the first-principles calculations. The Supporting Information is available free of charge on the ACS Publications website at DOI: 10.1021/jacs.5b03612.

AUTHOR INFORMATION

Corresponding Authors

*qunzh@ustc.edu.cn
*crwang@iccas.ac.cn
*yiluo@ustc.edu.cn

Author Contributions

‖B.W., J.H., and P.C. contributed equally.

Notes

The authors declare no competing financial interest.

ACKNOWLEDGMENTS

This work was jointly supported by the National Basic Research Program (2012CB932901 and 2010CB923300), National Natural Science Foundation of China (61227902, 51472248, 21273006, 21173205, 91127042, 20925311, and 11179006), the Key Research Program of the Chinese Academy of Sciences (KGZD-EW-T02), and the Strategic Priority Research Program B of the Chinese Academy of Sciences (XDB01020000).

REFERENCES

(1) Yannoni, C. S.; Hoinkis, M.; de Vries, M. S.; Bethune, D. S.; Salem, J. R.; Crowder, M. S.; Johnson, R. D. *Science* **1992**, *256*, 1191−1192.

(2) Rodriguez-Fortea, A.; Balch, A. L.; Poblet, J. M. *Chem. Soc. Rev.* **2011**, *40*, 3551−3563.

(3) Lu, X.; Akasaka, T.; Nagase, S. *Chem. Commun.* **2011**, *47*, 5942−5957.

(4) Dunsch, L.; Yang, S. F. *Phys. Chem. Chem. Phys.* **2007**, *9*, 3067−3081.

(5) Chaur, M. N.; Melin, F.; Ortiz, A. L.; Echegoyen, L. *Angew. Chem., Int. Ed.* **2009**, *48*, 7514−7538.

(6) Yamada, M.; Akasaka, T.; Nagase, S. *Acc. Chem. Res.* **2010**, *43*, 92−102.

(7) Popov, A. A.; Dunsch, L. *J. Am. Chem. Soc.* **2007**, *129*, 11835−11849.

(8) Kurihara, H.; Lu, X.; Iiduka, Y.; Nikawa, H.; Mizorogi, N.; Slanina, Z.; Tsuchiya, T.; Nagase, S.; Akasaka, T. *J. Am. Chem. Soc.* **2012**, *134*, 3139−3144.

(9) Maki, S.; Nishibori, E.; Terauchi, I.; Ishihara, M.; Aoyagi, S.; Sakata, M.; Takata, M.; Umemoto, H.; Inoue, T.; Shinohara, H. *J. Am. Chem. Soc.* **2012**, *135*, 918−923.

(10) Garcia-Borras, M.; Osuna, S.; Swart, M.; Luis, J. M.; Sola, M. *Angew. Chem., Int. Ed.* **2013**, *52*, 9275−9278.

(11) (a) Takano, Y.; Herranz, M. A.; Martin, N.; Radhakrishnan, S. G.; Guldi, D. M.; Tsuchiya, T.; Nagase, S.; Akasaka, T. *J. Am. Chem. Soc.* **2010**, *132*, 8048−8055. (b) Guldi, D. M.; Feng, L.; Radhakrishnan, S. G.; Nikawa, H.; Yamada, M.; Mizorogi, N.; Tsuchiya, T.; Akasaka, T.; Nagase, S.; Angeles Herranz, M.; Martin, N. *J. Am. Chem. Soc.* **2010**, *132*, 9078−9086. (c) Feng, L.; Radhakrishnan, S. G.; Mizorogi, N.; Slanina, Z.; Nikawa, H.; Tsuchiya, T.; Akasaka, T.; Nagase, S.; Martin, N.; Guldi, D. M. *J. Am. Chem. Soc.* **2011**, *133*, 7608−7618.

(12) Xenogiannopoulou, E.; Couris, S.; Koudoumas, E.; Tagmatarchis, N.; Inoue, T.; Shinohara, H. *Chem. Phys. Lett.* **2004**, *394*, 14−18.

(13) Yamada, M.; Akasaka, T.; Nagase, S. *Chem. Rev.* **2013**, *113*, 7209−7264.

(14) Lu, X.; Akasaka, T.; Nagase, S. *Acc. Chem. Res.* **2013**, *46*, 1627−1635.

(15) Wang, T.; Wang, C. *Acc. Chem. Res.* **2013**, *47*, 450−458.

(16) Rudolf, M.; Wolfrum, S.; Guldi, D. M.; Feng, L.; Tsuchiya, T.; Akasaka, T.; Echegoyen, L. *Chem.—Eur. J.* **2012**, *18*, 5136−5148.

(17) (a) Imahori, H.; Sakata, Y. *Adv. Mater.* **1997**, *9*, 537−546. (b) Guldi, D. M. *Chem. Commun.* **2000**, 321−327. (c) Guldi, D. M.; Prato, M. *Acc. Chem. Res.* **2000**, *33*, 695−703.

(18) Bottari, G.; de la Torre, G.; Guldi, D. M.; Torres, T. *Chem. Rev.* **2010**, *110*, 6768−6816.

(19) Rudolf, M.; Feng, L.; Slanina, Z.; Akasaka, T.; Nagase, S.; Guldi, D. M. *J. Am. Chem. Soc.* **2013**, *135*, 11165−11174.

(20) Feng, L.; Rudolf, M.; Wolfrum, S.; Troeger, A.; Slanina, Z.; Akasaka, T.; Nagase, S.; Martin, N.; Ameri, T.; Brabec, C. J.; Guldi, D. M. *J. Am. Chem. Soc.* **2012**, *134*, 12190−12197.

(21) (a) Takano, Y.; Obuchi, S.; Mizorogi, N.; Garca, R.; Herranz, M. A.; Rudolf, M.; Guldi, D. M.; Martin, N.; Nagase, S.; Akasaka, T. *J. Am. Chem. Soc.* **2012**, *134*, 19401−19408. (b) Takano, Y.; Obuchi, S.; Mizorogi, N.; Garcia, R.; Herranz, M. A.; Rudolf, M.; Wolfrum, S.; Guldi, D. M.; Martin, N.; Nagase, S.; Akasaka, T. *J. Am. Chem. Soc.* **2012**, *134*, 16103−16106.

(22) McCluskey, D. M.; Smith, T. N.; Madasu, P. K.; Coumbe, C. E.; Mackey, M. A.; Fulmer, P. A.; Wynne, J. H.; Stevenson, S.; Phillips, J. P. *ACS Appl. Mater. Interfaces* **2009**, *1*, 882−887.

DOI: 10.1021/jacs.5b03612
J. Am. Chem. Soc. 2015, 137, 8769−8774

(23) Zhang, J.; Stevenson, S.; Dorn, H. C. *Acc. Chem. Res.* **2013**, *46*, 1548−1557.
(24) Gust, D.; Moore, T. A.; Moore, A. L. *Acc. Chem. Res.* **2001**, *34*, 40−48.
(25) Ross, R. B.; Cardona, C. M.; Guldi, D. M.; Sankaranarayanan, S. G.; Reese, M. O.; Kopidakis, N.; Peet, J.; Walker, B.; Bazan, G. C.; Van Keuren, E.; Holloway, B. C.; Drees, M. *Nat. Mater.* **2009**, *8*, 208−212.
(26) Popov, A. A.; Yang, S.; Dunsch, L. *Chem. Rev.* **2013**, *113*, 5989−6113.
(27) Hannaford, P. *Femtosecond Laser Spectroscopy*; Springer: New York, 2005.
(28) Kroto, H. W.; Heath, J. R.; O'Brien, S. C.; Curl, R. F.; Smalley, R. E. *Nature* **1985**, *318*, 162−163.
(29) Inakuma, M.; Yamamoto, E.; Kai, T.; Wang, C.; Tomiyama, T.; Shinohara, H.; Dennis, T. J. S.; Hulman, M.; Krause, M.; Kuzmany, H. *J. Phys. Chem. B* **2000**, *104*, 5072−5077.
(30) Kurihara, H.; Lu, X.; Iiduka, Y.; Nikawa, H.; Hachiya, M.; Mizorogi, N.; Slanina, Z.; Tsuchiya, T.; Nagase, S.; Akasaka, T. *Inorg. Chem.* **2012**, *51*, 746−750.
(31) Lu, X.; Nakajima, K.; Iiduka, Y.; Nikawa, H.; Mizorogi, N.; Slanina, Z.; Tsuchiya, T.; Nagase, S.; Akasaka, T. *J. Am. Chem. Soc.* **2011**, *133*, 19553−19558.
(32) Lu, X.; Nakajima, K.; Iiduka, Y.; Nikawa, H.; Tsuchiya, T.; Mizorogi, N.; Slanina, Z.; Nagase, S.; Akasaka, T. *Angew. Chem., Int. Ed.* **2012**, *51*, 5889−5892.
(33) Iiduka, Y.; Wakahara, T.; Nakajima, K.; Tsuchiya, T.; Nakahodo, T.; Maeda, Y.; Akasaka, T.; Mizorogi, N.; Nagase, S. *Chem. Commun.* **2006**, 2057−2059.
(34) Iiduka, Y.; Wakahara, T.; Nakajima, K.; Nakahodo, T.; Tsuchiya, T.; Maeda, Y.; Akasaka, T.; Yoza, K.; Liu, M. T. H.; Mizorogi, N.; Nagase, S. *Angew. Chem., Int. Ed.* **2007**, *46*, 5562−5564.
(35) Yamazaki, Y.; Nakajima, K.; Wakahara, T.; Tsuchiya, T.; Ishitsuka, M. O.; Maeda, Y.; Akasaka, T.; Waelchli, M.; Mizorogi, N.; Nagase, S. *Angew. Chem., Int. Ed.* **2008**, *47*, 7905−7908.
(36) (a) Kasha, M. *Disc. Faraday Soc.* **1950**, *9*, 14−19. (b) Lakowicz, J. R. *Principles of Fluorescence Spectroscopy*; Springer: New York, 2006.
(37) (a) Goushi, K.; Yoshida, K.; Sato, K.; Adachi, C. *Nat. Photonics* **2012**, *6*, 253−258. (b) Uoyama, H.; Goushi, K.; Shizu, K.; Nomura, H.; Adachi, C. *Nature* **2012**, *492*, 234−238. (c) Sato, K.; Shizu, K.; Yoshimura, K.; Kawada, A.; Miyazaki, H.; Adachi, C. *Phys. Rev. Lett.* **2013**, *110*, 247401.
(38) Kurihara, H.; Lu, X.; Iiduka, Y.; Mizorogi, N.; Slanina, Z.; Tsuchiya, T.; Akasaka, T.; Nagase, S. *J. Am. Chem. Soc.* **2011**, *133*, 2382−2385.
(39) Cai, W.; Chen, M.; Bao, L.; Xie, Y.; Akasaka, T.; Lu, X. *Chem.—Eur. J.* **2015**, *21*, 3449−3454.

DOI: 10.1021/jacs.5b03612
J. Am. Chem. Soc. 2015, 137, 8769−8774